Imaging wave-penetrable objects in a finite depth ocean

Keji Liu[*]   Yongzhi Xu[†]   Jun Zou[‡]

Abstract. We extend the direct sampling method proposed in [13] to image a wave-penetrable inhomogeneous medium in a 3D waveguide. Incidences and receivers are available only on part of the surface of a cylinder. The proposed method is basically direct and does not involve any matrix inversions or optimizations, thus computationally very cheap and efficient. Numerical simulations are presented to show the feasibility and effectiveness of the method for acoustic detection in a 3D waveguide. The method is applicable with a few scattered fields corresponding to only one or two incident waves, and is very robust against noise.

Key words. Finite depth ocean, inhomogeneous media, direct sampling method.
MSC classifications. 35R30, 41A27, 76Q05.

1 Introduction

The direct and inverse scattering problems of underwater acoustics have received much attention in recent years, see, e.g., [1, 2, 4, 5, 7, 14, 15, 17] and the references therein. One of the popular models used for acoustic waves in a finite depth ocean is the waveguide bounded by two parallel planes. Because of the geometric structure, the inverse scattering problems in a parallel waveguide are much harder than similar problems in a homogeneous space. Due to the presence of two boundaries of the waveguide, only a finite number of wave modes can propagate in long distance, while the other modes decay exponentially as a function of distance. This phenomenon increases the ill-posedness of the inverse problem considerably. Assume that the ocean has a pressure released surface and a rigid bottom, we can pose a Dirichlet condition on one of the plane and a Neumann condition on the other. Based on this model, the exact and asymptotic representations of the sound field in a stratified shallow ocean was obtained in [3]. Adding a scatterer to the stratified model, a series of studies have been carried out for the direct and inverse scattering of acoustic waves by obstacles in a waveguide with plane boundaries as well as in an ocean under different sediment settings. We refer readers to [9, 10, 11, 6, 8, 12, 16, 19, 20] for more details.

In this paper we extend the direct sampling method proposed in [13] for imaging a wave-penetrable inhomogeneous medium in a 3D finite depth ocean. The method is based on a scattering analysis and involves only computing the inner product of the measured scattered field u^s

---

[*]Department of Mathematics, The Chinese University of Hong Kong, Shatin, Hong Kong. (`kjliu@math.cuhk.edu.hk`)

[†]Department of Mathematics, University of Louisville, Louisville, KY 40245, USA. (`ysxu0001@louisville.edu`)

[‡]Department of Mathematics, The Chinese University of Hong Kong, Shatin, Hong Kong. The work of this author was substantially supported by Hong Kong RGC grant (Project 404611). (`zou@math.cuhk.edu.hk`)

with fundamental solutions located at the sampling points over the measurement curve/surface. The method is basically direct and does not involve any matrix inversions or optimizations. Our numerical experiments indicate that it can provide an accurate and reliable estimate of the support of unknown scatterers, even in the presence of a fairly large amount of noise in the measured data. Consequently, it can be regarded as an effective but simple computational alternative to existing tools for locating a reliable approximate positions of the unknown obstacles, or for generating an initial sampling region for the use in a more refined or computationally more demanding optimization-type algorithm.

The new method applies a sampling-type technique, and resembles the linear sampling-type methods (LSM) [5, 6, 17, 20], but it differs significantly from these existing techniques. Firstly, it does not perform any matrix inversions, or solves ill-posed linear integral equations, thus is computationally cheap. Secondly, the novel method requires only a few (e.g., one or two) incident waves for reconstructing the locations of scatterers/inhomogeneities, whereas the others usually require the data from sufficiently many incidents in order to acquire a reasonable reconstruction. Lastly, the new method is highly tolerant to noise.

The paper is organized as follows. In Section 2, the direct scattering problem for the 3D waveguide is presented, along with some useful notations, properties and identities. In section 3, we generate an iterative method to solve the direct scattering problem of the 3D waveguide. Section 4 describes the mathematical motivation of the extended direct sampling method using the near-field data and proposes a new indicator function. Section 5 provides extensive numerical experiments to evaluate the performance of the novel indicator function by the near-field data from scatterers. Finally, some concluding remarks are stated in Section 6.

2   The direct scattering problem for the 3D waveguide

In this section, we describe the direct scattering problem of our interest. Consider a three-dimensional waveguide $\mathbb{R}_h^3 = \mathbb{R}^2 \times (0, h)$ for $h > 0$. The third coordinate axis is singled out as the one orthogonal to the waveguide, so we shall write

$$x = (x_1, x_2, x_3)^\top = (\tilde{x}, x_3)^\top \quad \forall\, x \in \mathbb{R}^3.$$

The upper and lower boundaries of the waveguide are denoted respectively by

$$\Gamma^+ := \{x \in \mathbb{R}^3;\ x_3 = h\} \quad \text{and} \quad \Gamma^- := \{x \in \mathbb{R}^3;\ x_3 = 0\}.$$

A bounded and wave-penetrable scatterer D is assumed to be compactly contained in the waveguide. The part of the waveguide not occupied by $\overline{D}$ is denoted by $\Omega := \mathbb{R}_h^3 \backslash \overline{D}$, which is assumed to be connected. Let us point out here that we shall often work later in the bounded domain $\Omega_R := \{x \in \Omega : |\tilde{x}|^2 < R^2\}$, where the radius R is assumed to be large enough such that $1 + |\tilde{x}|^2 < R^2$ for all $(\tilde{x}, x_3) \in D$. This implies that $\overline{D}$ is contained in the interior of Ω_R. The surface of the cylinder

$$\Gamma_R := \{x \in \Omega;\ |\tilde{x}|^2 = R^2\}$$

denotes the boundary of Ω_R that is contained in Ω. The two other parts of $\partial\Omega_R$, contained in the upper and lower boundaries of the waveguide, are denoted by

$$\Gamma_R^+ := \{x \in \mathbb{R}^3;\ |\tilde{x}| < R,\ x_3 = h\} \quad \text{and} \quad \Gamma_R^- := \{x \in \mathbb{R}^3;\ |\tilde{x}| < R,\ x_3 = 0\}.$$

Figure 1 shows a diagram of the waveguide's geometry.

The direct scattering of acoustic wave in a parallel waveguide with a wave-penetrable medium is modeled by the Helmholtz equation

$$\Delta u + k^2 n(x) u = f(x) \text{ in } \mathbb{R}_h^3, \tag{2.1}$$

where $u = u^i + u^s$, formed by the incident wave u^i and its corresponding scattered wave u^s. The sound-hard and sound-soft boundary conditions are imposed on the lower and upper boundaries of the waveguide, i.e.,

$$u = 0 \text{ on } \Gamma^- \quad \text{and} \quad \frac{\partial u}{\partial x_3} = 0 \text{ on } \Gamma^+. \tag{2.2}$$

The source function $f(x)$ has compact support, such that $supp(f) \cap \overline{D} = \emptyset$. We assume that the wave number $k > 0$, $q(x) = n(x) - 1 \geq 0$, and

$$supp(n(x) - 1) \equiv supp(q(x)) \subset D.$$

Consequently, it yields that $n(x) = 1$ for $x \notin D$ while $n(x) = 1 + q(x)$ for $x \in D$, with $q(x)$ called the contrast function. The incident wave u^i is a solution to the inhomogeneous Helmholtz equation with $n(x) \equiv 1$, which implies,

$$\Delta u^i + k^2 u^i = f(x). \tag{2.3}$$

The scattered wave $u^s = u - u^i$ satisfies the out-going radiation condition [9] for $x \in \Omega \backslash \overline{\Omega}_R$ and

$$u^s(x) = \sum_{m=1}^{\infty} \sin(\alpha_m x_3) u_m(\tilde{x}),$$

where $\alpha_m = \frac{(2m-1)\pi}{2h}$. The modes u_m are subject to the Sommerfield radiation condition [6]:

$$\lim_{r \to \infty} r^{1/2} \left(\frac{\partial u_m}{\partial r} - i k u_m \right) = 0, \tag{2.4}$$

uniformly for all $\tilde{x}$, with $r = |\tilde{x}|$.

We rewrite the equation (2.1) into the following form,

$$\Delta(u^s + u^i) + k^2 n(x)(u^s + u^i) = f(x),$$

which leads to

$$\Delta u^s + k^2(1 + q(x))u^s + \Delta u^i + k^2 u^i + k^2 q(x) u^i = f(x).$$

Hence, with the help of (2.3), we have the following equation

$$\Delta u^s + k^2(1 + q)u^s = -k^2 q u^i. \tag{2.5}$$

The Green's function [3] for the homogeneous medium $(n \equiv 1)$ in the waveguide $\mathbb{R}_h^3$ with the condition (2.2) is

$$G(x, y) = \frac{i}{2h} \sum_{m=1}^{\infty} \sin(\alpha_m x_3) \sin(\alpha_m y_3) H_0^{(1)}(k_m |\tilde{x} - \tilde{y}|), \quad x, y \in \Omega, \ \tilde{x} \neq \tilde{y}, \tag{2.6}$$

3

where $k_m = \sqrt{k^2 - \alpha_m^2}$. An equivalent representation of the Green's function in (2.6) can be derived via the method of images,

$$G(x, y) = \frac{1}{4\pi} \sum_{m=-\infty}^{+\infty} (-1)^m \left\{ \frac{e^{ik|x-y_m|}}{|x - y_m|} - \frac{e^{ik|x-y_m'|}}{|x - y_m'|} \right\}, \tag{2.7}$$

where the source image points are given by

$$y_m = (y_1, y_2, y_3)^\top + (0, 0, 2mh) \quad \text{and} \quad y_m' = (y_1, y_2, -y_3) + (0, 0, 2mh), \quad m \in \mathbb{Z}.$$

From the formula (2.7), it is obvious that $G(\cdot, \cdot)$ can be written as the superposition of the fundamental solution $\Phi(x - y) = e^{ik|x-y|}/(4\pi|x - y|)$ of the Helmholtz equation in free space and an analytic function $\tilde{G}(\cdot, \cdot)$, that is,

$$G(x, y) = \frac{1}{4\pi} \frac{e^{ik|x-y|}}{|x - y|} + \tilde{G}(x, y), \quad x \neq y \in \Omega. \tag{2.8}$$

Accordingly, the mapping properties of the volume potential

$$\int_D G(\cdot, y) f(y) dy$$

are the same as for the volume potential with kernel

$$\Phi = \frac{1}{4\pi} \frac{e^{ik|x-y|}}{|x - y|}.$$

From (2.5) we derive,

$$\Delta u^s + k^2 u^s = -k^2 q u^s - k^2 q u^i,$$

then we can represent the scattered field u^s and the total field u as

$$u^s(x) = k^2 \int_D G(x, y) q(y) u(y) dy, \quad x \in \mathbb{R}_h^3 \tag{2.9}$$

and

$$u(x) = k^2 \int_D G(x, y) q(y) u(y) dy + u^i(x), \quad x \in \mathbb{R}_h^3. \tag{2.10}$$

Suppose that the incident wave is a point source wave from x_s, say, $f(x) = -\delta(x - x_s)$, then

$$u^i(x, x_s) = G(x, x_s).$$

The formula (2.10) indicates that the total field $u(x)$ satisfies the integral equation,

$$u(x) = k^2 \int_D G(x, y) q(y) u(y) dy + G(x, x_s), \quad x \in D. \tag{2.11}$$

Since the operator

$$Su(x) := k^2 \int_D G(x, y) q(y) u(y) dy, \quad x \in D$$

is compact in $L^2(D)$, (2.11) is uniquely solvable for

$$k^2 \int_D |G(x, y) q(y)|^2 dy < 1. \tag{2.12}$$

After we obtain the total field $u(x)$ for $x \in D$, the scattered field $u^s(x)$ for $x \in \mathbb{R}_h^3$ can be straightforwardly generated by the formula (2.9).

3   An iterative algorithm for the direct scattering problem

As we know, the near-field or scattered data is obtained through some measurements in practical applications. But for the verification of the effectiveness of a reconstruction method, we need to generate the scattered data by solving the direct scattering problem. In this section, we propose a simple iterative method for solving the direct scattering problem of the shallow ocean waveguide. Suppose some scatterers are embedded in the cylinder Ω_R with the refractive index $n(x) \neq 1$. We choose a few arc segments with the central angle α of some circles on the surface of cylinder Ω_R, see Γ_s and Γ_r in Figure 2. Some source points x_s are located at Γ_s, see the red star points in Figure 2, and a set of receivers x_r are situated at Γ_r, see the blue circle points in Figure 2.

Assume that the condition (2.12) is satisfied, we first solve the volume integral (2.11) iteratively for $x \in D$. Let $u_1(x) = G(x, x_s)$,

$$u_{n+1}(x) = k^2 \int_D G(x, y) q(y) u_n(y) dy + G(x, x_s), \quad n = 1, 2, \cdots. \tag{3.1}$$

For the implementation of this iterative method, we discretize the scatterer D into N small cubes and the center point of each cube is denoted as y_m for $1 \leq m \leq N$. Therefore, we obtain the following formula from (3.1):

$$u_{n+1}(x_m) = k^2 \sum_{p=1}^{N} G(x_m, y_p) A q(y_p) u_n(y_p) + G(x_m, x_s), \quad m = 1, 2, \cdots, N, \tag{3.2}$$

where A is the volume of each cube.

With the total field $u(x)$ obtained for $x \in D$, we can compute the scattered field $u^s(x_r)$ by

$$u^s(x_r) = k^2 \int_D G(x_r, y) q(y) u(y) dy, \quad x_r \in \Gamma_r, \tag{3.3}$$

or approximately by

$$u^s(x_r) = k^2 \sum_{p=1}^{N} G(x_r, y_p) A q(y_p) u(y_p), \quad x_r \in \Gamma_r. \tag{3.4}$$

4   A direct sampling method for the inverse scattering problem

In this section, we attempt to extend the direct sampling method proposed in [13] to determine a stable and accurate approximation to the shape of inhomogeneities in our interested 3D waveguide model with a finite depth. Here is an explicit statement of the the inverse problem to be considered in this work, namely to determine the supports of inhomogeneities D from the scattered field u^s measured on Γ_r.

Now we would like to derive an index function which has significantly different behaviors inside and outside the scatterers. The derivation is carried out for a cylindrical surface Γ_R; see Figure 1. Let $G(x, x_p)$ be the fundamental solution associated with the Helmholtz equation in the waveguide $\mathbb{R}_h^3$:

$$\Delta G(x, x_p) + k^2 G(x, x_p) = -\delta(x - x_p) \tag{4.1}$$

with two boundary conditions $G = 0$ on Γ^- and $\frac{\partial G}{\partial x_3} = 0$ on Γ^+, where $\delta(x - x_p)$ refers to the Dirac delta function located at the point $x_p \in \Omega_R$. Multiplying both sides of the equation (4.1) by the conjugate $\overline{G}(x, x_q)$ of the fundamental solution $G(x, x_q)$ and integrating over the domain Ω_R, we have

$$\int_{\Omega_R} (\Delta G(x, x_p) + k^2 G(x, x_p))\overline{G}(x, x_q)dx = -\overline{G}(x_p, x_q). \tag{4.2}$$

Next we consider the equation (4.1) with $x_q \in \Omega_R$ in place of x_p, and take its conjugate. Then multiplying both sides of the resulting equation by $G(x, x_p)$ and integrating over the domain Ω_R, we obtain

$$\int_{\Omega_R} (\Delta\overline{G}(x, x_q) + k^2\overline{G}(x, x_q))G(x, x_p)dx = -G(x_p, x_q). \tag{4.3}$$

Applying integration by parts for the terms involving Laplacians in (4.2) and (4.3), we can deduce that

$$
\begin{aligned}
2i\mathrm{Im}\Big(G(x_p, x_q)\Big) &= G(x_p, x_q) - \overline{G}(x_p, x_q) \tag{4.4}\\[2mm]
&= \int_{\Gamma_R} \left[\overline{G}(x, x_q)\frac{\partial G(x, x_p)}{\partial n} - G(x, x_p)\frac{\partial\overline{G}(x, x_q)}{\partial n}\right]dS,
\end{aligned}
$$

where Im means the imaginary part of a complex quantity. Note that $\frac{\partial G}{\partial n}(x, x_p) = \frac{\partial G}{\partial r}(x, x_p)$, we readily derive

$$
\begin{aligned}
\frac{\partial G}{\partial n}(x, x_p) &= \frac{\partial}{\partial r}\left[\sum_{m=1}^{\infty} \frac{i}{2h}\sin(\alpha_m x_3)\sin(\alpha_m(x_p)_3)H_0^{(1)}(k_m|\tilde{x} - \tilde{x}_p|)\right]\\[2mm]
&= \sum_{m=1}^{\infty} \frac{i}{2h}\sin(\alpha_m x_3)\sin(\alpha_m(x_p)_3)\frac{\partial}{\partial r}H_0^{(1)}(k_m|\tilde{x} - \tilde{x}_p|)\\[2mm]
&= \sum_{m=1}^{\infty} \frac{i}{2h}\sin(\alpha_m x_3)\sin(\alpha_m(x_p)_3)\left[ik_m H_0^{(1)}(k_m|\tilde{x} - \tilde{x}_p|) + \mathcal{O}\left(\frac{1}{r^3}\right)\right].
\end{aligned}
$$

Similarly,

$$\frac{\partial\overline{G}}{\partial n}(x, x_q) = \sum_{m=1}^{\infty} \frac{-i}{2h}\sin(\alpha_m x_3)\sin(\alpha_m(x_p)_3)\left[-ik_m\overline{H}_0^{(1)}(k_m|\tilde{x} - \tilde{x}_q|) + \mathcal{O}\left(\frac{1}{r^3}\right)\right].$$

6

Therefore, with the help of (4.4),

$$2i\mathrm{Im}\Big(G(x_p, x_q)\Big)$$

$$= 2i\mathrm{Im}\Big(\sum_{m=1}^{\infty}\frac{i}{2h}\sin(\alpha_m(x_p)_3)\sin(\alpha_m(x_q)_3)H_0^{(1)}(k_m|\tilde{x}_p - \tilde{x}_q|)\Big)$$

$$= \int_{\Gamma_R}\Big[\overline{G}(x, x_q)\frac{\partial G}{\partial n}(x, x_p) - G(x, x_p)\frac{\partial \overline{G}}{\partial n}(x, x_q)\Big]dS$$

$$= \int_{|\tilde{x}|=R}\int_0^h\Big[\overline{G}(x, x_q)\frac{\partial G}{\partial n}(x, x_p) - G(x, x_p)\frac{\partial \overline{G}}{\partial n}(x, x_q)\Big]dx_3 ds(\tilde{x})$$

$$\approx \int_{|\tilde{x}|=R}\sum_{m=1}^{\infty}\frac{ik_m}{8h}\sin(\alpha_m(x_p)_3)\sin(\alpha_m(x_q)_3)\cdot\Big[H_0^{(1)}(k_m|\tilde{x} - \tilde{x}_p|)\overline{H}_0^{(1)}(k_m|\tilde{x} - \tilde{x}_q|)$$

$$+ \overline{H}_0^{(1)}(k_m|\tilde{x} - \tilde{x}_q|)H_0^{(1)}(k_m|\tilde{x} - \tilde{x}_p|)\Big]ds(\tilde{x}).$$

Accordingly, we arrive at the following approximation for $m = 1, 2, \cdots$,

$$\frac{ik_m}{8h}\int_{|\tilde{x}|=R}H_0^{(1)}(k_m|\tilde{x} - \tilde{x}_p|)\overline{H}_0^{(1)}(k_m|\tilde{x} - \tilde{x}_q|)ds(\tilde{x}) \approx \frac{2i}{h}\mathrm{Im}\Big(\frac{i}{2}H_0^{(1)}(k_m|\tilde{x}_p - \tilde{x}_q|)\Big).$$

Now we consider a sampling region $\tilde{D}$ that contains the scatterer D. In order to implement the novel method, the domain $\tilde{D}$ is divided into a set of small elements $\{\tau_j\}$. Let $W(y) = k^2 q(y)u(y)$, then by the rectangular quadrature rule we obtain the following simple approximation of the scattered field

$$u^s(x) = \int_{\tilde{D}}G(x, y)W(y)dy \approx \sum_j w_j G(x, y_j),$$

where the point y_j is in the jth element τ_j, and the weight w_j is given by $w_j = aW(y_j)$ for a being the volume of the element τ_j and $W(y_j) = k^2 q(y_j)u(y_j)$.

Now we consider the following integral on the surface Γ_R,

$$\int_{\Gamma_R} u^s(x)\overline{G}(x,x_p)dS$$

$$= \int_{\Gamma_R}\int_{\tilde{D}} G(x,y)W(y)dy\,\overline{G}(x,x_p)dS$$

$$= \int_{\tilde{D}}\left[\int_{\Gamma_R} G(x,y)\overline{G}(x,x_p)ds\right]W(y)dy$$

$$= \int_{\tilde{D}} W(y)\left(\int_{|\tilde{x}|=R}\int_0^h \sum_{m=1}^\infty \frac{i}{2h}\sin(\alpha_m x_3)\sin(\alpha_m y_3)H_0^{(1)}(k_m|\tilde{x}-\tilde{y}|)\right.$$

$$\left.\cdot \sum_{n=1}^\infty \frac{i}{2h}\sin(\alpha_n x_3)\sin(\alpha_n(x_p)_3)H_0^{(1)}(k_n|\tilde{x}-\tilde{x}_p|)dx_3 ds(\tilde{x})\right)dy$$

$$= \int_{\tilde{D}} W(y)\left[\sum_{m=1}^\infty \frac{-1}{4h^2}\int_{|\tilde{x}|=R}\frac{h}{2}\sin(\alpha_m y_3)\sin(\alpha_m(x_p)_3)H_0^{(1)}(k_m|\tilde{x}-\tilde{y}|)\right.$$

$$\left.\cdot H_0^{(1)}(k_m|\tilde{x}-\tilde{x}_p|)ds(\tilde{x})\right]dy$$

$$= \int_{\tilde{D}} W(y)\left[\sum_{m=1}^\infty \frac{-1}{4h^2}\cdot\frac{h}{2}\sin(\alpha_m y_3)\sin(\alpha_m(x_p)_3)\int_{|\tilde{x}|=R}H_0^{(1)}(k_m|\tilde{x}-\tilde{y}|)\right.$$

$$\left.\cdot H_0^{(1)}(k_m|\tilde{x}-\tilde{x}_p|)ds(\tilde{x})\right]dy$$

$$\approx \int_{\tilde{D}} W(y)\left\{\sum_{m=1}^\infty \frac{-1}{8h}\sin(\alpha_m y_3)\sin(\alpha_m x_{p3})\cdot\frac{16}{k_m}\mathrm{Im}\left(\frac{i}{2}H_0^{(1)}(k_m|\tilde{y}-\tilde{x}_p|)\right)\right\}dy.$$

Hence, we accomplish the following approximation,

$$\int_{\Gamma_R} u^s(x)\overline{G}(x,x_p)ds \approx \sum_j w_j \mathrm{Im}\left(\hat{G}(y_j,x_p)\right), \tag{4.5}$$

where

$$\hat{G}(y_j,x_p) = \sum_{m=1}^\infty -\frac{2}{h}\cdot\frac{1}{k_m}\sin(\alpha_m y_3)\sin(\alpha_m(x_p)_3)\cdot\left[\frac{i}{2}H_0^{(1)}(k_m|\tilde{y}_j-\tilde{x}_p|)\right].$$

We notice that if x_p is far away from all physical point scatterers $\{y_j\}$, then the summation in (4.5) will be relative small due to decay property of the fundamental solution $G(x,y)$. On the contrary, if a point x_p is close to some physical point scatterer $y_j \in D$, then $\hat{G}(y_j,x_p)$ takes a relative large value and thus contributes significantly to the sum. Moreover, if the radius R of Ω_R is large, $G(y_j,x_p)$ and $\hat{G}(y_j,x_p)$ can be approximated by the sums of the propagating modes. In summary, all these facts lead us to the following index function

$$I(x_p) = \frac{|\langle u^s, G(\cdot,x_p)\rangle_{L^2(\Gamma_R)}|}{||u^s||_{L^2(\Gamma_R)}||G(\cdot,x_p)||_{L^2(\Gamma_R)}} \quad \forall\, x_p \in \tilde{D}, \tag{4.6}$$

8

with
$$\langle u^s, G(\cdot, x_p)\rangle_{L^2(\Gamma_R)} = \int_{\Gamma_R} u^s(x)\overline{G}(x, x_p)ds.$$

When there are several sets of scattered data available, we shall extend the above index function I to the formula
$$I(x_p) = \max_i\{I_i(x_p)\} \quad \forall\, x_p \in \tilde{D}, \tag{4.7}$$

where I_i refers to the index function (4.6) defined for the ith data set.

In practice, $I(x_p) \approx 1$ implies that the sampling point x_p lies most likely inside the support of a scatterer, while $I(x_p) \approx 0$ indicates that the sampling point lies outside the support of any scatterer component. Hence, the indicator function I provides the likelihood of the sampling point x_p lying inside the supports of scatterers. No unstable matrix inversion as in the LSM is needed for estimating the index function I. The indicator function I involves only evaluating the inner product of the scattered field and the fundamental solution, thus computational very cheap. Moreover, the data noise enters the index function I through the integration of the measured data u^s on the boundary Γ_R. The subsequent numerical simulations will demonstrate the feasibility and effectiveness of the new method as well as its robustness with respect to the noise in the data.

5   Numerical Simulation

In this section, we are going to present a few numerical examples to evaluate the feasibility and effectiveness of the direct sampling method based on the index function (4.6) or (4.7). In our numerical simulations, the sampling region $\tilde{D}$ is chosen to be $[-1, 1] \times [-1, 1] \times [2, 4]$, the height h of the shallow water is 8, the wavenumber k is 6, the Green's function (2.6) is truncated at $100th$ term. The incident fields will be specified for each example, and the corresponding scattered filed u^s is measured at the following points that are uniformly distributed on the specified circles with the angle step size $h_a = \frac{\pi}{12}$:

$$x = 5\cos(\theta),\ y = 5\sin(\theta),\ z = 1 + 0.4(n-1), \quad \theta = 0, h_a, \cdots, 2\pi;\ n = 1, 2, \cdots, 11.$$

We first apply the iterative method proposed in Section 3 to generate the scattered data u^s and terminate the iteration when the relative L^2-norm error of the field is less than $\varepsilon = 10^{-3}$. Then the noisy data u^s_δ is generated pointwise by the formula

$$u^s_\delta(x) = u^s(x) + \varepsilon\delta(x)\max_x|u^s(x)|,$$

where ε refers to the relative noise level, and both the real and imaginary parts of the noise $\delta(x)$ follow the standard normal distribution. The mesh size for the forward problem is chosen to be 0.02, while the one for the inverse problem is 0.05. The medium contrast function q of the scatterer is 1 for all the following experiments. The index function (4.6) for estimating the contrast q is normalized so that its maximum value is 1, and it will be displayed in each numerical simulation. If it is not specified, the cut-off value 0.5 is used for the index function values $I(x)$ in numerical examples, namely, all the sampling points x_p satisfying $I(x_p) < 0.5$ will be dropped in forming the reconstructed scatterers.

Example 1 We consider a scatterer occupying the region $(-0.2, 0.2) \times (-0.2, 0.2) \times (2.8, 3.2)$. Only 1 source point, located at $(5\cos\frac{\pi}{4}, 5\sin\frac{\pi}{4}, 6)$, is employed in this numerical experiment.

The numerical reconstructed scatterer is shown in Figure 3, with a relative noise level being $\varepsilon = 10\%, 20\%$ and 30% respectively. As we may observe that the index I is relatively large at the sampling points close to the physical scatterer, otherwise it is relatively small. The reconstructed scatterer is given in Figure 4, with reconstructed locations and shapes being quite reasonable even with noise level up to 30%, considering the fact that only one source point is used for the numerical reconstruction. So the new sampling method appears to be very robust against noise.

Example 2 This example investigates two separated scatterers occupying the regions $(-0.8, -0.4) \times (-0.8, -0.4) \times (2.2, 2.6)$ and $(0.4, 0.8) \times (0.4, 0.8) \times (3.4, .3.8)$ respectively. Only 2 source points are applied, at the locations $(5\cos\frac{\pi}{4}, 5\sin\frac{\pi}{4}, 6)$ and $(5\cos\frac{3\pi}{4}, 5\sin\frac{3\pi}{4}, 6)$ respectively.

For the ease of the illustration and observation, we only plot the values of the index function I in the regions $(-1, -0.2) \times (-1, -0.2) \times (2, 2.8)$ and $(0.2, 1) \times (0.2, 1) \times (3.2, 4)$. Figure 5 shows the index value distributions and Figure 6 plots the reconstructed scatterers, with the relative noise level ε being $10\%, 20\%$ and 30% respectively.

We observe that the support estimated by the indicator function I agrees very well with the exact one, and the index values decrease quickly away from the boundary of the true scatterers. So the sampling method works also well for multiple scatterer components. But due to the physical scattering interaction between the two scatterer components, we can observethat the left lower object has an extra part on the right-hand side while the right upper object has an extra part on the left-hand side.

Example 3 This example concerns the reconstruction of two very close scatterers occupying the regions $(-0.6, -0.2) \times (-0.2, 0.2) \times (2.8, 3.2)$ and $(0.2, 0.6) \times (-0.2, 0.2) \times (2.8, .3.2)$ respectively. The same two source points are used as in Example 2. The reconstructions are shown in Figure 7 for the distributions of the index function $I(x)$ and in Figure 8 for the approximate scatterers, with the relative noise level ε being $10\%, 20\%$ and 30% respectively.

As we may observe, the two scatterers stay very close to each other in this example, less than one half of the wavelength in distance, which is known to be rather challenging in numerical reconstruction. Nonetheless, both scatterers are clearly seen separated and the approximate locations of the scatterers are still rather impressive, considering only two point sources were employed. But due to the physical scattering interaction between the two close scatterer components, we can observe some artifact in each object grown towards the other one.

Example 4 In this final test, we consider a torus scatterer which has the following representation,

$$\left(R - \sqrt{x^2 + y^2}\right)^2 + z^2 = r^2,$$

where $r = 0.1$ and $R = 0.4$ (R is the radius from the center of the hole to the center of torus tube, r is the radius of the tube). Only 6 source points are employed in this experiment, which are located at $(5\cos\frac{\pi}{3}, 5\sin\frac{\pi}{3}, 6)$, $(5\cos\frac{2\pi}{3}, 5\sin\frac{2\pi}{3}, 6)$, $(5\cos\pi, 5\sin\pi, 6)$, $(5\cos\frac{4\pi}{3}, 5\sin\frac{4\pi}{3}, 6)$, $(5\cos\frac{5\pi}{3}, 5\sin\frac{5\pi}{3}, 6)$ and $(5\cos 2\pi, 5\sin 2\pi, 6)$ respectively.

The reconstructions are shown in Figure 9 for the distributions of the index function $I(x)$ and in Figure 10 for the approximate scatterers, with the relative noise level ε being $1\%, 5\%$ and 10% respectively and the cut-off value c being 0.7.

The torus scatterer represents one of the most challenging scatterers to recover, and it is highly nontrivial even with multiple data sets, especially noting that the diameter of the torus

less than one half of the wavelength. Nonetheless, the new sampling method seems to be able to provide a quite reasonable estimate of the shape of the torus.

6   Concluding remarks

We have extended the direct sampling method proposed in [13] to image wave-penetrable inhomogeneous media in a 3D waveguide. The method involves only the inner product of the scattered field with the fundamental solutions at the sampling points over some curves where the scattered field is measured, without any optimizations or matrix inversions required. So it is basically a direct method. The method is applicable to give reasonable reconstructions of scatterers with a very limited amount of measured data corresponding to only few incident waves. Moreover, the algorithm is easy to implement, computationally very cheap and highly tolerant to noise. Consequently, it can serve as an efficient yet simple computational alternative to provide a reasonable initial sampling domain for the use in existing more accurate and more refined optimization-type reconstruction algorithms.

Acknowledgements

References

[1] T. Arens, D. Gintides and A. Lechleiter, *Variational formulations for scattering in a 3-dimensional acoustic waveguide*, Math. Methods Appl. Sci. **31** 821-847, 2008.

[2] T. Arens, D. Gintides and A. Lechleiter, *Direct and inverse medium scattering in a three-dimensional homogeneous planar waveguide*, SIAM J. Appl. Math., **71** 753-772, 2011.

[3] D. Ahluwalia and J. Keller, *Exact and asymptotic representations of the sound field in a stratified ocean*, in Wave Propagation and Underwater Acoustics, Lecture Notes in Phys. **70**, Springer, Berlin 14-85, 1977.

[4] L. Bourgeois, C. Chambeyron and S. Kusiak, *Locating an obstacle in a 3d finite depth ocean using the convex scattering support*, J. Comput. Appl. Math., **204** 387-399, 2007.

[5] L. Bourgeois and E. Lunéville, *The linear sampling method in a waveguide: a modal formulation*, Inv. Prob. **24** (2008), 015018 (20pp).

[6] J. Buchanan, R. Gilbert, A. Wirgin and Y. Xu, *Marine Acoustics: Direct and Inverse Problems*, SIAM, Philadelphia, 2004.

[7] S. Dediu and J. Mclaughlin, *Recovering inhomogeneities in a waveguide using eigensystem decomposition*, Inv. Prob. **22** 1227-1246, 2006.

[8] R. Gilbert, M. Wirby and Y. Xu, *Determination of a buried object in a two-layered shallow ocean*, J. Comput. Acoust. **9** 1025-1037, 2001.

[9] R. GILBERT AND Y. XU, *Dense sets and the projection theorem for acoustic waves in a homogeneous finite depth ocean*, Math. Methods Appl. Sci. **12** 67-76, 1989.

[10] R. GILBERT AND Y. XU, *Starting fields and far fields in ocean acoustics*, Wave Motion **11** 507-524, 1989.

[11] R. GILBERT AND Y. XU, *Acoustic imaging in a shallow ocean with a thin ice cap*, Inv. Prob. **16** 1799-811, 2000.

[12] R. GILBERT AND Y. XU, *The propagation problem and far-field pattern in a stratified finite-depth ocean*, Math. Methods Appl. Sci. **12** 199-208, 2005.

[13] K. ITO, B. JIN AND J. ZOU, *A direct sampling method to an inverse medium scattering problem*, Inv. Prob., **28** (2012), 025003 (11pp).

[14] M. IKEHATA, G. MAKRAKIS AND G. NAKAMURA, *Inverse boundary value problem for ocean acoustics using point sources*, Math. Methods Appl. Sci. **27** 1367-1384, 2004.

[15] A. LECHLEITER AND D. NGUYEN, *Spectral Volumetric Integral Equation Methods for Acoustic Medium Scattering in a Planar Homogeneous 3D Wave Guide*, preprint, 2010.

[16] D. LEE AND R. GILBERT, *Identification of objects in an acoustic wave guide inversion II: Robin-Dirichlet conditions*, Math. Methods Appl. Sci. **29** 401-414, 2006.

[17] K. LIU, Y. XU AND J. ZOU, *A Paralle Radial Bisection Algorihtm for Inverse Scattering Problems*, Inv. Prob. Sci. Eng., **21** 197-209, 2012.

[18] K. LIU AND J. ZOU, *A Multilevel Sampling Algorithm for Locating Inhomogeneous Media*, Inv. Prob., **29** (2013), 095003 (19pp).

[19] Y. XU, *The propagation solutions and far-field patterns for acoustic harmonic waves in a finite depth ocean*, Appl. Anal. **35** 129-151, 1990.

[20] Y. XU, C. MAWATA AND W. LIN, *Generalized dual space indicator method for underwater imaging*, Inv. Prob. **16** 1761-1776, 2000.

List of figures:

Figure 1. Geometrical illustration of the waveguide.

Figure 2. Geometrical illustration of the source points and receivers.
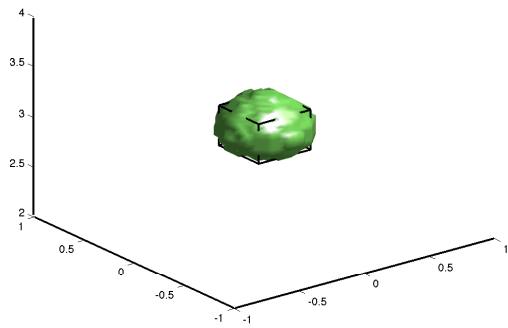
Figure 3. Exact contrast values $q(x)$ (a), and distributions of the index function $I(x)$ with $10\,\%$ noise (b), $20\,\%$ noise (c) and $30\,\%$ noise (d) for Example 1.
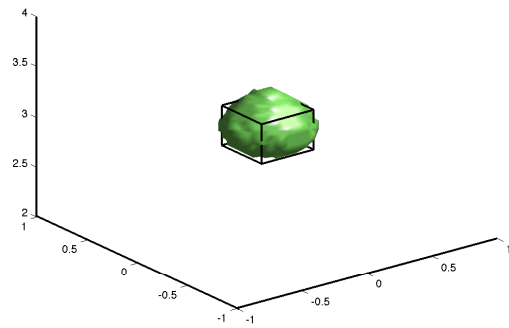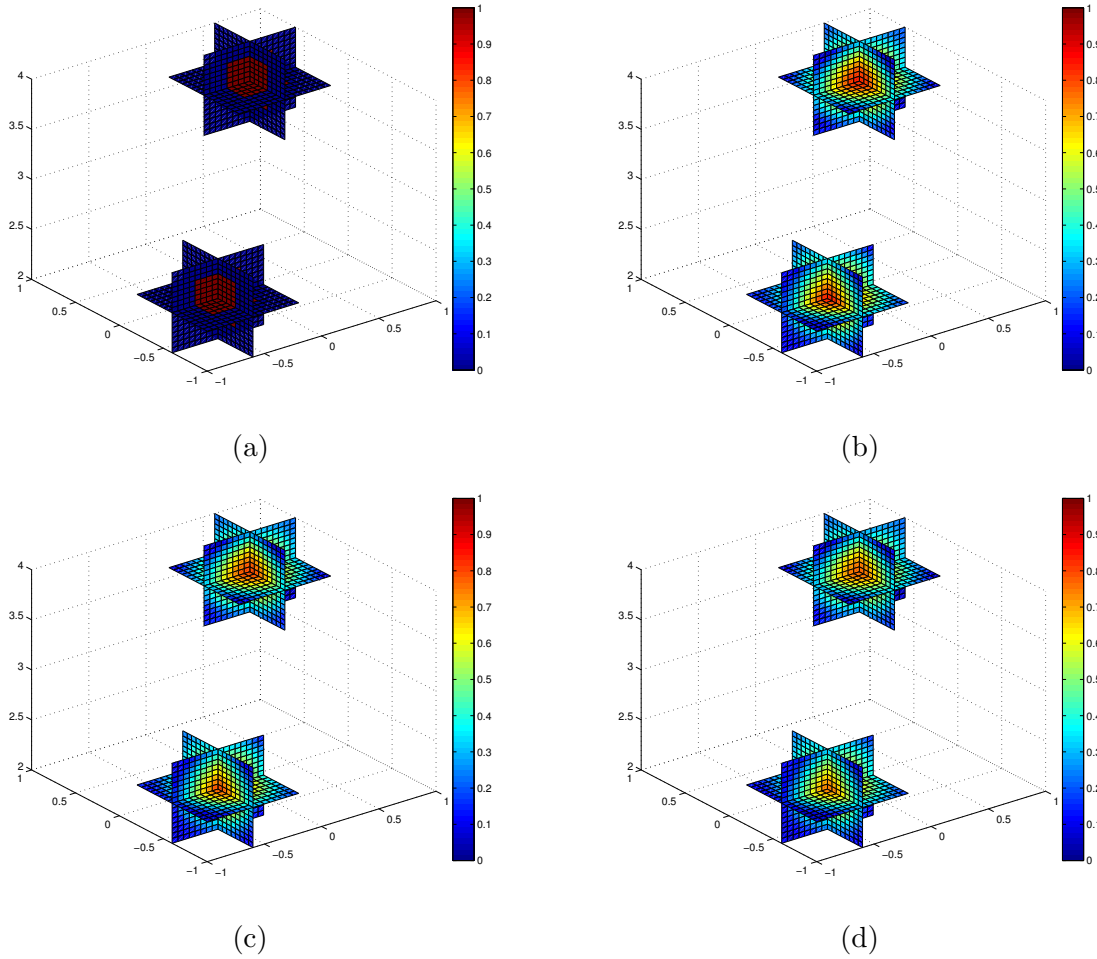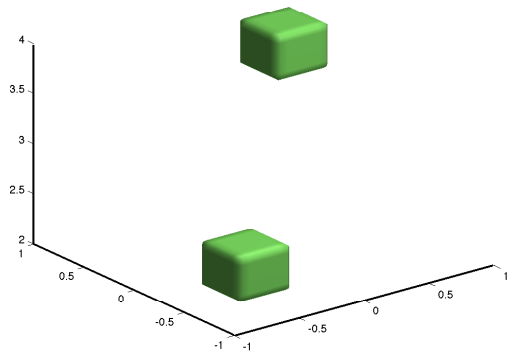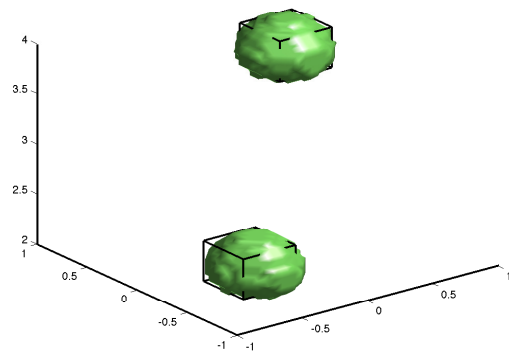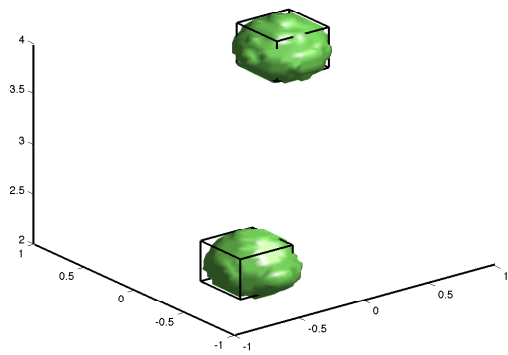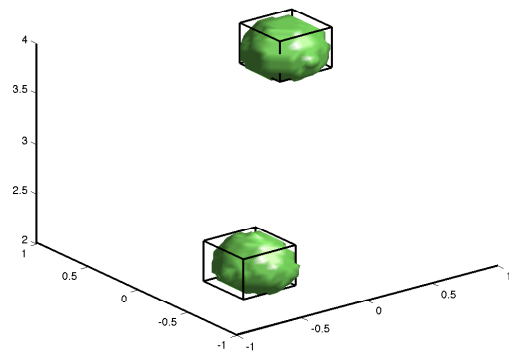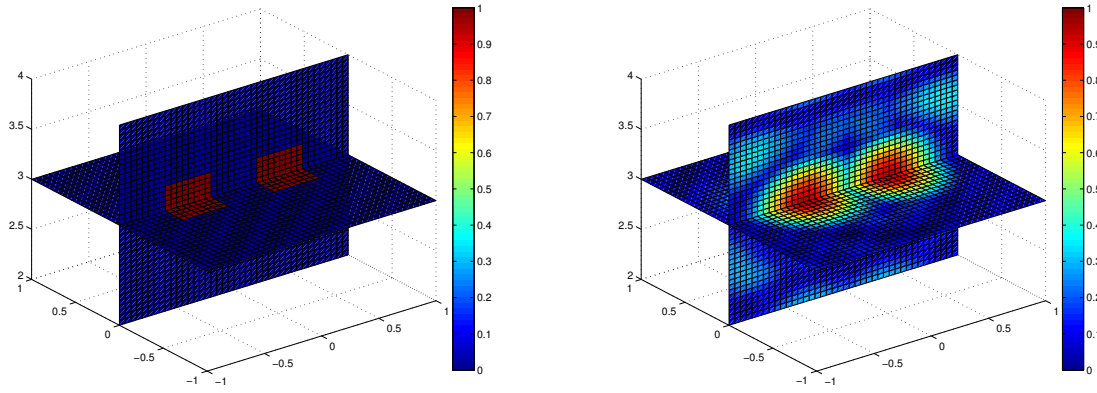
Figure 4. Exact scatterer (a), and reconstructed ones with $10\,\%$ noise (b), $20\,\%$ noise (c) and $30\,\%$ noise (d) for Example 1.

Figure 5. Exact contrast values $q(x)$ (a), and distributions of the index function $I(x)$ with $10\,\%$ noise (b), $20\,\%$ noise (c) and $30\,\%$ noise (d) for Example 2.

Figure 6. Exact scatterer (a), and reconstructed ones with $10\,\%$ noise (b), $20\,\%$ noise (c) and $30\,\%$ noise (d) for Example 2.

Figure 7. Exact contrast values $q(x)$ (a), and distributions of the index function $I(x)$ with $10\,\%$ noise (b), $20\,\%$ noise (c) and $30\,\%$ noise (d) for Example 3.

Figure 8. Exact scatterer (a), and reconstructed ones with $10\,\%$ noise (b), $20\,\%$ noise (c) and $30\,\%$ noise (d) for Example 3.

Figure 9. Exact contrast values $q(x)$ (a), and distributions of the index function $I(x)$ with $1\,\%$ noise (b), $5\,\%$ noise (c) and $10\,\%$ noise (d) for Example 4.

Figure 10. Exact scatterer (a), and reconstructed ones with $1\,\%$ noise (b), $5\,\%$ noise (c) and $10\,\%$ noise (d) for Example 4.

Figure 1: *Geometrical illustration of the waveguide.*
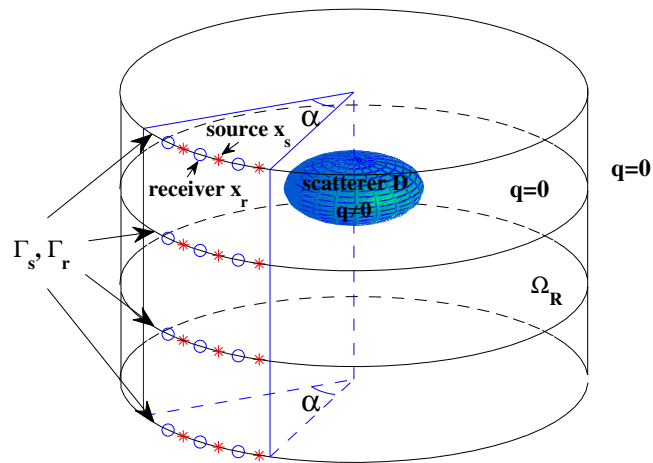
Figure 2: *Geometrical illustration of the source points and receivers.*

Figure 3: *Exact contrast values $q(x)$ (a), and distributions of the index function $I(x)$ with 10% noise (b), 20% noise (c) and 30% noise (d) for Example 1.*
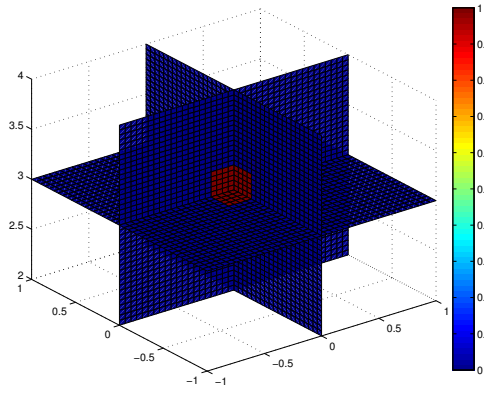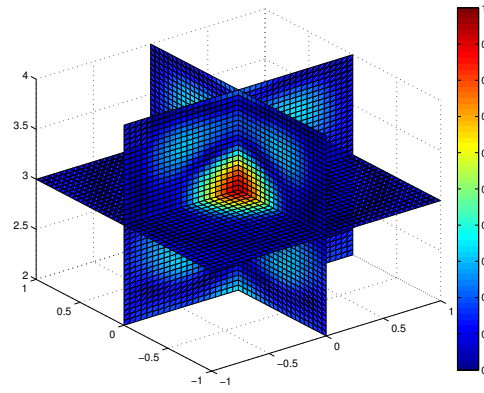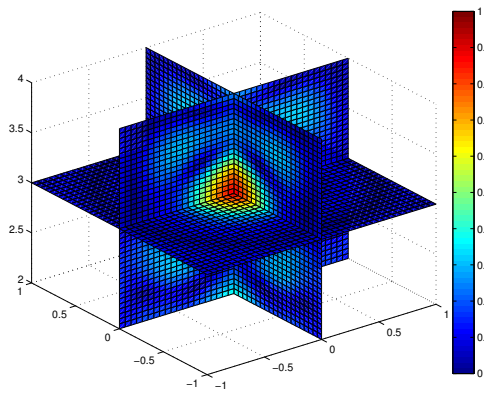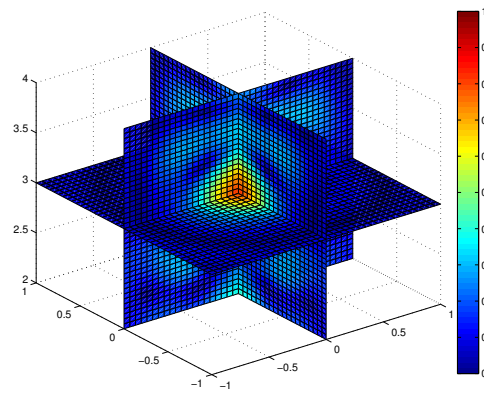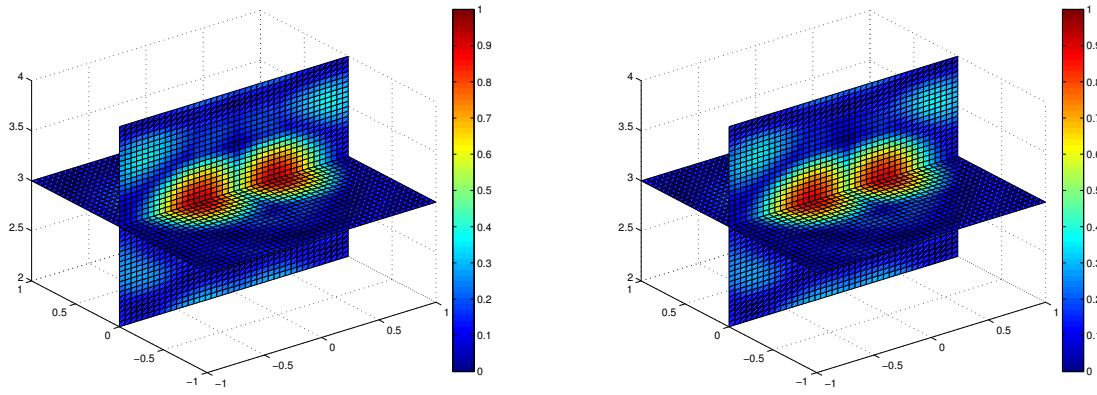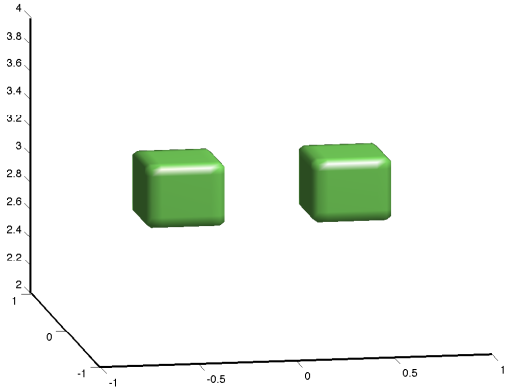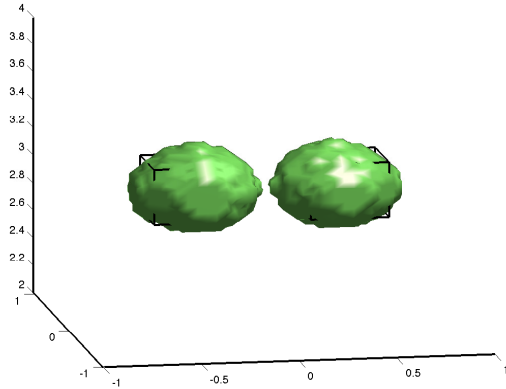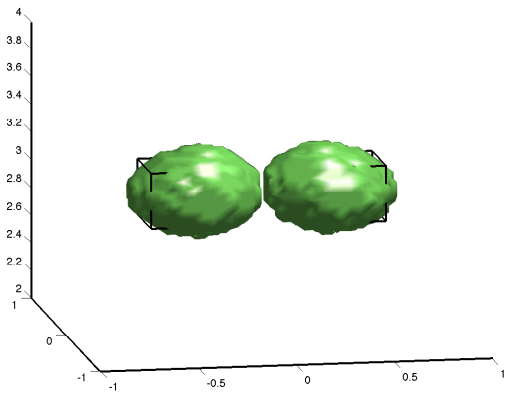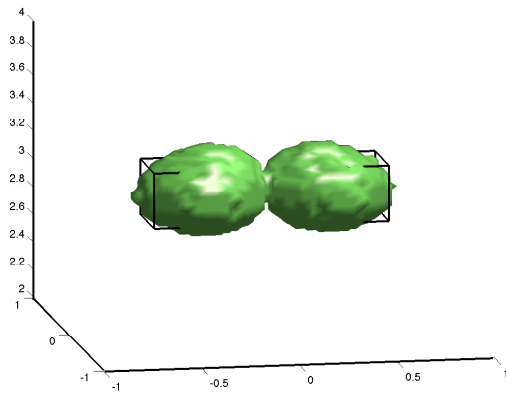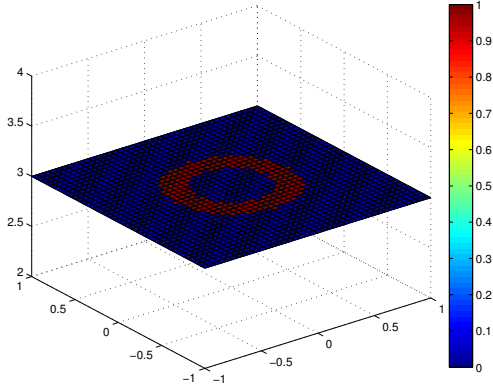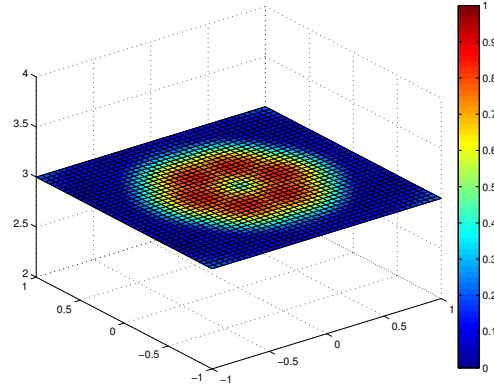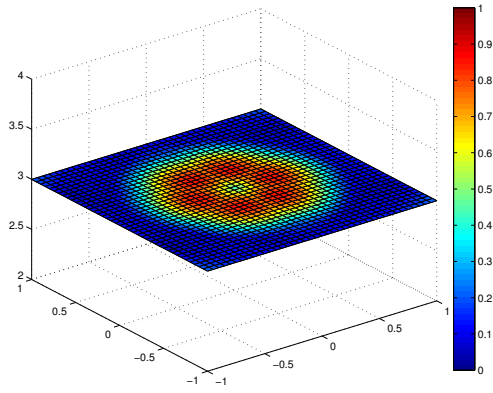
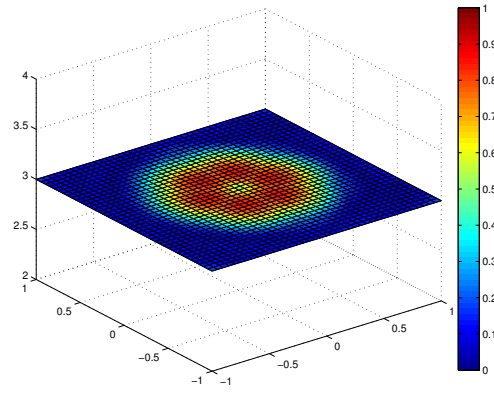Figure 4: *Exact scatterer (a), and reconstructed ones with 10% noise (b), 20% noise (c) and 30% noise (d) for Example 1.*
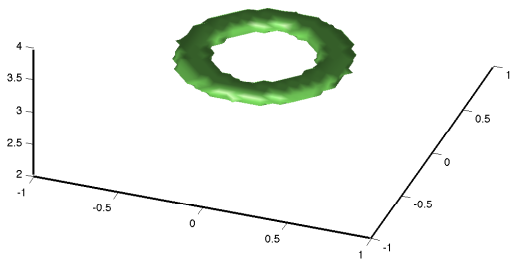
(a)

(b)

(c)

(d)

Figure 5: *Exact contrast values q(x) (a), and distributions of the index function I(x) with 10% noise (b), 20% noise (c) and 30% noise (d) for Example 2.*

17

(a)

(b)

(c)

(d)

Figure 6: *Exact scatterer (a), and reconstructed ones with 10% noise (b), 20% noise (c) and 30% noise (d) for Example 2.*
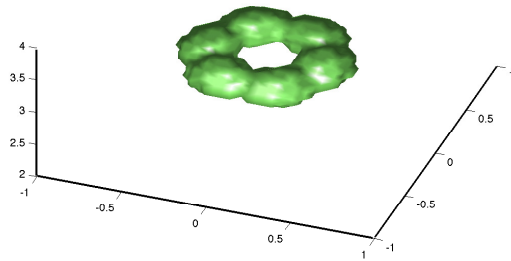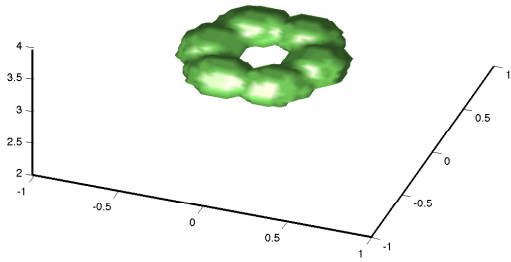
Figure 7: *Exact contrast values $q(x)$ (a), and distributions of the index function $I(x)$ with 10% noise (b), 20% noise (c) and 30% noise (d) for Example 3.*

Figure 8: *Exact scatterer (a), and reconstructed ones with 10% noise (b), 20% noise (c) and 30% noise (d) for Example 3.*

Figure 9: *Exact contrast values q(x) (a), and distributions of the index function I(x) with 1% noise (b), 5% noise (c) and 10% noise (d) for Example 4.*
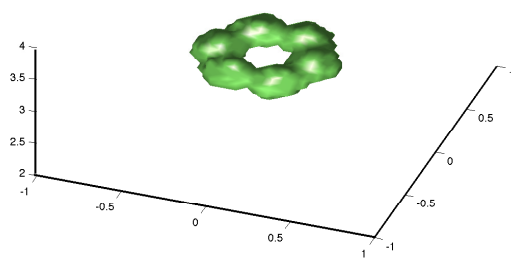
Figure 10: *Exact scatterer (a), and reconstructed ones with 1% noise (b), 5% noise (c) and 10% noise (d) for Example 4.*